ISSN 0454－4641

運輸省港湾技術研究所

港湾技術研究所報告

REPORT OF THE PORT AND HARBOUR RESEARCH INSTITUTE

MINISTRY OF TRANSPORT

VOL.39 NO.2 June 2000

NAGASE, YOKOSUKA, JAPAN

港湾技術研究所報告　(REPORT OF P. H. R. I.)

第39巻　第2号 (Vol. 39, No. 2), 2000年6月 (June 2000)

目　次 (CONTENTS)

REPORT OF THE PORT AND
HARBOUR RESEARCH INSTITUTE
Vol.39, No.2 (June 2000)

Numerical Study on the Flow Characteristics of Tide-Induced Jet

Jong-Chun PARK *
Tomonari OKADA **
Keita FURUKAWA ***
Keisuke NAKAYAMA **
Yasushi HOSOKAWA ****

Synopsis

The tide-induced jets over constant bathymetry are investigated in oscillating flow using a finite-difference numerical scheme, named NS-MAC-TIDE based on the fully 3D Navier-Stokes (NS) equations. In order to generate a jet in a tide-like oscillating flow, an enclosed rectangular breakwater, which has vertical opening and a large enclosed volume inside, known as a Tidal-Jet Generator (TJG), is introduced into a flow. During both phases of tide, strong and uni-directional jets can be obtained locally from the inlet of the TJG, due to the water level difference between the inner and outer sides of breakwater.

The computed results are extensively compared with three other independently developed numerical models, namely, 3D-ADI, DVM, and CIP-CSF. These models are based on quasi-three-dimensional, two-dimensional depth-averaged and fully three-dimensional NS equations, respectively. It is apparent that the fully three-dimensional numerical models can predict the maximum intensity of inlet velocity with high accuracy compared with the empirical function proposed from the experiments by Furukawa et al. (1994). It is also obvious that the numerical simulations can reproduce successfully the processes of generation, development and dissipation of tide-induced jets.

Key Words: Tidal-Jet Generator (TJG), tidal jet, fully 3D Navier-Stokes equation, finite-difference method, wave-height function, opening ratio, residual flow, Subgrid scale (SGS) turbulence model, water purification

* Visiting Scientist of Environmental Assessment Laboratory, Marine Environment Division
** Research Engineer of Environmental Assessment Laboratory, Marine Environment Division
*** Senior Research Engineer of Environment Purification Laboratory, Marine Environment Division
**** Chief of Environmental Assessment Laboratory, Marine Environment Division
3-1-1 Nagase, Yokosuka, 239-0826 Japan
Phone: +81-468-44-5018 Fax: +81-468-44-6243 e-mail: okada@cc.phri.go.jp

港湾技術研究所報告
第 39 巻第 2 号(2000.6)

潮汐噴流の流れ特性に関する数値的研究

朴　鍾千*・岡田　知也**・古川　恵太***・中山　恵介**・細川　恭史****

要　　旨

海域を小さな開口部を残すように防波堤で囲い込むと，潮汐運動に伴う海水の流動によって，開口部近傍での流れは噴流となる．このような造流堤（TJG）は前面海域における物質循環や移送過程を変化させ，滞留時間は減少すると考えられる．この TJG によって発生する潮汐噴流の基礎的流れ特性を数値的に解析するために，厳密な３次元のナビエ・ストークス方程式を解くことのできる NS-MAC-TIDE 法を適用し，その数値解法としての特徴を検討した．

本研究で開発された NS-MAC-TIDE 法と３種類の異なる数値計算法(3D-ADI 法、離散渦法(DVM)，CIP-CSF 法）により造流堤開口部における最大流速を各々推定し，水理模型実験結果と比較した．ここで，NS-MAC-TIDE 法と CIP-CSF 法はナビエ・ストークス方程式の厳密な３次元解法であるのに対し，3D-ADI は静水圧近似の３次元解法，DVM は水深平均値を用いた２次元解法である．TJG の開口率が小さく潮汐噴流が強い計算条件の下では，水深方向の現象が単純化された計算方法である 3D-ADI や DVM は実験結果を正確に再現することができないが，厳密な３次元解法である NS-MAC-TIDE 法および CIP-CSF 法は実験結果を正確に再現することができることが示された．

また，NS-MAC-TIDE 法を用いた計算結果から次のことが示された．①TJG により発生する噴流は，下げ潮の前半では加速噴流，後半には減速噴流と噴流の特性は大きく変化し，下げ潮や上げ潮速度最大時に低層において，はっきりとした接地境界層が形成されている．②TJG 周辺におけるせん断流速の計算結果から，粒子に対する底面から上方への拡散の強化，掃流力の空間的な急変による掘れおよび堆積の発生に関して定量的な評価を行うことが可能となった．③TJG の前面海域における物質循環や移送過程を再現するため濃度拡散のシミュレーションを行い，それらの滞留時間を数値的に予測することができた．これらの検討は，実験や観測によって推定することは精度上困難であり，NS-MAC-TIDE 法による成果である．

こうした検討により，本研究で適用した NS-MAC-TIDE 法は，潮汐噴流の生成・発達・逸散等の物理的プロセスを再現することができる方法の一つであり，流れ場の詳細な構造などを理解するために有効であることが示された．

キーワード：造流提，潮汐噴流，３次元 NS 方程式，有限差分法，波高関数，開口率，残差流，SGS 乱流モデル，海域浄化

*　海洋環境部 環境評価研究室 客員研究員
**　海洋環境部 環境評価研究室 研究官
***　海洋環境部 主任研究官
****　海洋環境部 環境評価研究室長
〒239-0826 横須賀市長瀬 3-1-1 運輸省港湾技術研究所
電話: 0468-44-5018　Fax: 0468-44-6243　e-mail: okada@cc.phri.go.jp

CONTENTS

1. Introduction

In the vicinity of tidal inlets such as estuary, river/bay mouths and port entrances, tide-induced currents are significant to coastal and marine environmental engineering. Furthermore, in the presence of a narrow entrance, currents can produce a strong and uni-directional localized jet flow in the neighborhood of such a sudden constriction. Such a jet is known as a tide-induced jet (or tidal jet) when it is due solely to the tidal forcing. During both phases of the tide, the flow issuing from the inlet forms a turbulent jet and generates eddy pairs of high vorticity near the head of jet. The large-eddy vortex pair created by the jet entrains the surrounding waters; consequently affecting the water mass distribution and transport processes in the domain of influence of the jet. Momentum dissipation in the jet grows gradually as the flow develops, due to the influence of vorticity at the head of the jet. These hydromechanical processes are repeated persistently on both sides of the inlet, with a period equal to that of the tide. Consequent effects on sediment and mass transport phenomena are to be expected.

A number of investigations (French, 1960, Taylor and Dean, 1974, Ozsoy, 1977, Unluata and Ozsoy, 1977, Joshi, 1982, Joshi and Taylor, 1983, Ismail and Wiegel, 1983, Wolanski et al., 1988) have been made to obtain the general solution for jet width and centerline velocity variations of fully-developed jets under the assumptions of self-similarity and quasi-steady turbulent jet behavior. However, these solutions do not cover one case of fundamental interest, which is to evaluate the maximum intensity of a starting jet before development occurs. This case is of interest because it will directly influence the flow patterns and structures in the area neighboring a narrow entrance. If a bay has a very thin vertical opening, tidal forcing may give rise to a large difference in surface elevation between the two sides of the entrance. Dissipation should be enhanced by strong water jets falling down through the inlet, and three-dimensional effects such as upwelling motion in the near field of inlet may be experienced.

In the present study, such tide-induced jets over constant bathymetry are investigated numerically. In order to generate a jet in a tide-like oscillating flow, an enclosed rectangular breakwater, which has vertical opening and a large enclosed volume inside, known as a Tidal-Jet Generator (TJG) (Furukawa et al., 1994), is introduced into a flow. The TJG is installed at the head of a rectangular bay. The forcing tide is given by imposing a sinusoidally varying water level at the entrance of bay. During both phases of tide, strong and uni-directional jets can be obtained locally from the inlet of the TJG, due to the water level difference between the inner and outer sides of breakwater.

The maximum intensity of the jets are numerically predicted and the relating processes of the jets are reproduced using a finite-differencing scheme, named NS-MAC-TIDE method, based on the fully three-dimensional Navier-Stokes (NS) equations and a modified Marker and Cell (MAC) algorithm. Boundary values are updated at each time step by a finite-difference time-marching scheme in the framework of a rectangular coordinate system. The Poisson equation for the pressure is solved iteratively using the Richardson method. Free-surface movement is satisfied by the dynamic and kinematic conditions.

The computed results are extensively compared with three other independently developed numerical models, namely, 3D-ADI method (Leendertse, 1989, Furukawa and Hosokawa, 1994), Discrete Vortex Method (Furukawa and Wolanski, 1998), and CIP-CSF method (Nakayama and Satoh, 1999). These models are based on quasi-three-dimensional, two-dimensional depth-averaged and fully three-dimensional NS equations, respectively. Through the comparison between the numerical models, cross-checks and identification of three-dimensional flow effects are examined. The fully three-dimensional NS-MAC-TIDE simulations are also compared with the hydraulic experiments (Furukawa et al., 1994). It is apparent that the fully three-dimensional numerical models can predict the maximum intensity of inlet velocity with high accuracy compared with the empirical function proposed from the experiment. It is seen that the horizontal area and the water depth are important parameters in deciding the optimal opening ratio of the system. It is also obvious that the numerical simulations can reproduce successfully the processes of generation, development and dissipation of tide-induced jets.

2. Finite Difference Method, NS-MAC-TIDE

2.1. Governing Equation

Assuming that the fluid is incompressible and homogeneous, the governing equations are given by the following NS equation and continuity equation:

$$\frac{\partial \mathbf{u}}{\partial t} = -\nabla\left(\frac{p}{\rho} + \frac{2}{3}k\right) + \mathbf{a}, \tag{1}$$

$$\nabla \mathbf{u} = 0, \tag{2}$$

where,

$$\mathbf{a} = -(\mathbf{u}\cdot\nabla)\mathbf{u} + (\nu + \nu_S)\nabla^2\mathbf{u} + (\nabla\nu_S)S + \mathbf{f}, \tag{3}$$

$$S = \begin{bmatrix} 2\dfrac{\partial u}{\partial x} & \dfrac{\partial u}{\partial y}+\dfrac{\partial v}{\partial x} & \dfrac{\partial u}{\partial z}+\dfrac{\partial w}{\partial x} \\ \dfrac{\partial v}{\partial x}+\dfrac{\partial u}{\partial y} & 2\dfrac{\partial v}{\partial y} & \dfrac{\partial v}{\partial z}+\dfrac{\partial w}{\partial y} \\ \dfrac{\partial w}{\partial x}+\dfrac{\partial u}{\partial z} & \dfrac{\partial w}{\partial y}+\dfrac{\partial v}{\partial z} & 2\dfrac{\partial w}{\partial z} \end{bmatrix}. \tag{4}$$

In the above equations, $\mathbf{u}=(u,v,w)$ is the velocity vector, p the pressure, t the time, ∇ the gradient operator, ν the kinematic viscosity for laminar flow, ν_S the eddy viscosity coefficient of the subgrid-scale (SGS) turbulence model, and $\mathbf{f}$ is the external force including the gravitational acceleration. The density ρ is assumed constant over the fluid region. The SGS turbulence model is introduced in the same manner in Miyata and Yamada (1992). According to the Smagorinsky et al.'s assumption (1965) the SGS eddy viscosity ν_S and the turbulent kinetic energy k are derived as, respectively

$$\nu_S = (C_1\Delta)^2\left[\frac{\partial u_i}{\partial x_j}\left(\frac{\partial u_i}{\partial x_j}+\frac{\partial u_j}{\partial x_i}\right)\right]^{1/2}, \tag{5}$$

$$k = \frac{(\nu_S)^2}{(C_0\Delta)^2}, \tag{6}$$

where, C_1=0.1 and C_0=0.094 for the present study, and Δ is the length scale set at $\Delta=(\Delta x\Delta y\Delta z)^{1/3}$.

In the time-marching procedure, the solutions of the governing equations in each region are obtained separately at each time step. At the free surface, the following kinematic and dynamic conditions can be applied neglecting viscous stress and surface tension:

$$\frac{D(\eta - z)}{Dt} = 0, \tag{7}$$

$$p = p_{\text{air}}. \tag{8}$$

Here, D is the total derivative, η denotes the free-surface profile, so-called the wave-height function, and z represents the vertical coordinate. Equation (7) means that the particle on the free-surface moves with the free-surface. After determining the free-surface location, the governing equation (1) is integrated in the computational domain.

2.2 Algorithm and Differencing Scheme

The solution algorithm is similar in substance to the NS-MAC-NWT (Park et al., 1999) and the TUMMAC method (Park and Miyata, 1994, Miyata and Park, 1995) in which the velocity and pressure points are defined in a staggered

manner in the framework of a rectangular coordinate system. In the time-marching process, the distribution of wave height is calculated from equation (7) and the new pressure field is determined by iteratively solving the following Poisson equation:

$$\nabla \cdot \nabla P = \nabla \cdot \left(\mathbf{a} + \frac{\mathbf{u}^{(n)}}{\Delta t} \right) = \nabla \cdot \mathbf{b}\,, \tag{9}$$

$$P^{m+1} = P^{m} + \omega_0 \left(\nabla \cdot \nabla P - \nabla \cdot \mathbf{b} \right), \tag{10}$$

where, $P=p/\rho$, and ω_0 is the relaxation factor set at a value smaller than unity. The superscript n denotes the time level and m the iteration level. The **b** term includes both diffusion and convection terms and is called the source term. The velocity field is updated through the NS equation (1) and the boundary values of the velocities are then set at the new location of the interface. The NS equation (1) is hyperbolic equations to be solved as an initial-value problem, while the Poisson equation (9) is an elliptic equation to be solved as a boundary-value problem. Equation (1) is solved by time-marching and at every time step equation (9) is solved by an iterative procedure. The cycle is repeated until the number of time steps reaches the predetermined final value.

The finite-difference scheme for the convective terms must be carefully chosen, since it often renders decisive influences on the results. In the present simulation, for the convective term a flux-split method such like a third-order upwind scheme with variable mesh size is employed in space so that variable mesh system can be used for all three directions. The second-order Adams-Bashforth method is used for the time-differencing. On the other hand, a second-order central differencing scheme is employed for the diffusive terms.

The transport equation (5) of wave-height function is approximated by a fully-implicit method:

$$a_p \eta_{ij}^{n+1} = a_e \eta_{i+1j}^{n+1} + a_w \eta_{i-1j}^{n+1} + a_n \eta_{ij+1}^{n+1} + a_s \eta_{ij-1}^{n+1} + c\,, \tag{11}$$

where,

$$a_e = -\frac{\Delta t \left(u_p - |u_p| \right)}{2\Delta x_{i+1/2}}, \tag{12a}$$

$$a_w = \frac{\Delta t \left(u_p + |u_p| \right)}{2\Delta x_{i-1/2}}, \tag{12b}$$

$$a_n = -\frac{\Delta t \left(v_p - |v_p| \right)}{2\Delta y_{j+1/2}}, \tag{12c}$$

$$a_s = \frac{\Delta t \left(v_p + |v_p| \right)}{2\Delta y_{j-1/2}}, \tag{12d}$$

$$a_p = \left(1 + a_e + a_w + a_n + a_s \right), \tag{12e}$$

$$c = \eta_{ij}^{n} + w_p \Delta t\,. \tag{12f}$$

Here, the subscript (i,j) indicates the discretized location of wave-height. The solution of discretization equation (11) can be obtained by standard Gaussian-elimination.

The dynamic free-surface condition of equation (8) is implemented by the so-called "irregular star" technique (Chan and Street, 1970) in the solution process of the Poisson equation for the pressure. The pressure at the free-surface is determined by extrapolating with zero gradient in a direction approximately normal to the free surface and taking into

Table 1 Characteristics of Various Numerical Models

	NS-MAC-TIDE	3D-ADI	DVM	CIP-CSF
Discretization	FDM	FDM	DVM	FDM
Governing Eq.	Fully 3D NS	3D NS using hydrostatic assumption	2D depth-averaged NS	Fully 3D NS
Grid System	Rectangular	Rectangular	—	Curvilinear
Calculation Point	Staggered mesh	Staggered mesh	Released vortex points (Lagrangian)	Staggered mesh
Time Integration	Explicit (2nd-order Adams-Bashforth)	ADI	Explicit (Euler)	Explicit (Euler)
Differencing of Convective Term	3rd-order upwind	3rd-order upwind	Lagrangian	CIP
Eddy Viscosity	by SGS model	Constant (0-equation)	Implicit (Vortex core)	by SGS model
Boundary Condition (BC) of Free-surface (Kinematic)	Wave-height Function Eq.	Depth-averaged continuity Eq.	Depth-averaged continuity Eq.	ALE
BC on Vertical Wall	No-slip	No-slip	Slip	No-slip

consideration the static pressure difference in the vertical direction due to gravity. Similarly, velocities are extrapolated at the interface with approximately no normal gradient. This treatment is in gross accord with the viscous tangential condition at the free surface.

2.3 Other Boundary Conditions

The no-slip boundary condition is imposed on enclosed solid walls including the breakwater. All velocity components are set to zero on the boundary, while the pressure and the values of wave height are extrapolated by applying the no-normal-gradient condition in horizontal direction. In the vertical direction, however, pressure is extrapolated by considering the static pressure differences.

A forcing tide at the open boundary is given by:

$$\eta = A\cos\left(\frac{2\pi}{T}t\right) = A\cos\sigma t\,, \tag{13}$$

where, A is the amplitude, T the period of tide, σ the angular frequency of tide, and t the time. The forcing tide will be started from a maximum ebb tide. The static pressure is set at the open boundary according to the time-movement of sea level given in equation (13).

3. Other Numerical Models

The computational results for the application of the NS-MAC-TIDE to the tidal jet are compared with the other three independently developed numerical models; 3D-ADI, DVM, and CIP-CSF. The characteristics of the other numerical models are described briefly in this section and are summarized in **Table 1**.

3.1 3D-ADI Method

This finite-difference model for the computation of three-dimensional free-surface flows solves the continuity and the NS equations using the hydrostatic assumption for pressure in the vertical. With this assumption, the momentum equations to be solved become:

$$\frac{\partial \phi}{\partial t}+u\frac{\partial \phi}{\partial x}+v\frac{\partial \phi}{\partial y}+w\frac{\partial \phi}{\partial z}=-\frac{1}{\rho}\nabla P+\nu_h\left(\frac{\partial^2 \phi}{\partial x^2}+\frac{\partial^2 \phi}{\partial y^2}\right)+\nu_z\left(\frac{\partial^2 \phi}{\partial z^2}\right), \tag{14}$$

$$\frac{\partial P}{\partial z}=-\rho g, \tag{15}$$

where, ν_h and ν_z are the horizontal and the vertical eddy diffusivity, respectively. In equation (14) above, the dependent variable ϕ represents repeatedly the horizontal velocity components, u and v.

A three-dimensional ADI (Alternated Directions Implicit) algorithm (Leendertse, 1989, Furukawa and Hosokawa, 1994) is introduced in the time-marching procedure, which allows the calculation of a three-dimensional system with large timesteps to be stable and not to be constrained by surface wave propagation.

3.2 Discrete Vortex Method (DVM)

The DVM is based on the two-dimensional depth-averaged NS equation and the conservative equation. The model has been adapted for use under the boundary element method (BEM) to account for solid boundaries (Kuwahara, 1978).

In a coordinate system moving with the circulation Γ, defined as $\Gamma \equiv \int_S \omega \, \mathrm{d}S$, where, ω is the vorticity, S the area disturbed by the vorticity, the governing equations are simplified to:

$$\frac{\mathrm{d}\Gamma}{\mathrm{d}t}=-\gamma_b\frac{|\mathbf{u}|}{h}\Gamma+K_X\nabla^2\Gamma, \tag{16}$$

where, h the water depth, K_X the horizontal eddy viscosity coefficient, and γ_b the bottom friction coefficient initially taken to be equivalent to Manning's friction coefficient.

The left-hand side in equation (16) represents the rate of change of the circulation along the path of the discrete vortex, the first term of right-hand side represents the effect of bottom friction, and the second term, the diffusion of vorticity. The development of the circulation due to an individual vortex of circulation Γ is calculated using a Lagrangian method. A vortex is assumed to have a core which has Gaussian distribution of vorticity:

$$\omega=\frac{\Gamma}{\pi d^2}\exp\left(-\frac{r^2}{d^2}\right), \tag{17}$$

where r is the distance from the center and d is the diameter of the vortex core where induced velocity becomes maximum. As a result of diffusion, d is assumed to increase with time as following:

$$d=\sqrt{4K_X t}\ . \tag{18}$$

The tangential velocity u_r induced by this vortex is

$$u_r=\frac{\Gamma}{2\pi r}\left[1-\exp\left(-\frac{r^2}{4K_X t}\right)\right]. \tag{19}$$

The details of solution algorithm are described in Furukawa and Wolanski (1998).

3.3 CIP-CSF Method

The CIP-CSF method has been developed and applied to perform large-eddy simulations (LES) of gravity currents in a stratified field.

The Boussinesq approximation is introduced in the governing equations: the fully three-dimensional momentum and continuity equations, and the diffusion equations for temperature and salinity. In the present study, however, the effect of stratification is negligible and the momentum and continuity equations only are solved over the flow field. The curvilinear grid system is used for fitting not only to the topography but also to the water-surface. The governing equations are discretized in a manner of the finite-differencing scheme that employs an explicit time-marching procedure with the SGS turbulence model for stratification (Schmidt and Schumann, 1989).

The movement of the water-surface is updated using the ALE method (Hirt et al., 1972). The pressure and velocity are solved by means of a simultaneous iterative method, the so-called HSMAC-type algorithm by Hirt et al. (1975). The convective terms are discretized using the CIP method (Yabe et al, 1990).

Full details of the solution algorithm are contained in Nakayama and Satoh (1999).

4. Computational Results and Discussions

4.1 Tidal-Jet Generator (TJG) Model

In the design of a TJG, flow separation due to sudden contraction and expansion of the entrance is expected to be the primary physical feature. For analytical simplicity, the barriers are assumed to be thin and vertical. As depicted in **Figure 1**, the TJG model is installed at the head of a rectangular bay whose depth (h) is shallow and constant. The coordinate system has its origin at the center of the inlet. The head of bay is a reflecting wall and the no-slip boundary condition is imposed here. Tidal forcing is given by imposing a sinusoidally varying water level from equation (13) at the entrance of bay. It is assumed that the incoming tide; is sufficiently long compared to the depth and the width of bay; is of small amplitude; and is normally incident to the entrance of bay. Thus, the long tidal waves should be regarded as propagating with the shallow water wave celerity $C_W=\sqrt{gh}$, where g is the gravity acceleration. Furthermore, wave reflections are assumed insignificant in the system.

During both phases of the tide, the strong and uni-directional tide-induced jets are generated locally through the inlet, due to the water level difference between the inner and outer sides of breakwater. At any one time, the inlet acts as a potential source to one side and a sink of equal magnitude to the other. This locally-induced jet flow can decrease the residence time of a pollutant distributed around the outside of inlet on the ebb tide. This jet effect utilizes tidal energy to influence the local marine environment by providing a flushing mechanism for water purification.

In such a system, it has been shown that two parameters can be used to characterize both experimental and numerical results. One parameter is the opening ratio ε defined as $\varepsilon = \varepsilon_0 h/S$, where ε_0 is the opening between the adjacent slots of barrier and S ($=B\times L$) the horizontal area inside the breakwater. Here, it is seen that the horizontal area and the water depth are important parameters in deciding the optimal opening ratio of the system. The other one is the maximum intensity of inlet velocity U_{max}, which is newly defined here as $U_{max} = U/\sigma A$, where U is the maximum inlet velocity.

4.2 Numerical Convergence Tests of the NS-MAC-TIDE Simulation

First, numerical convergence tests of the NS-MAC-TIDE simulation were carried out in a rectangular bay with length and width l=8.75 (m) and b=10 (m), respectively. The model was adjusted to agree with the experiments by Furukawa et al. (1994). Computations were made over a range of CFL numbers denoted by $C_w\cdot\Delta t/\Delta z$. All other parameters were constant for each case at T=390 (sec), $2A$=0.0037 (m), S=2.01(=1.15×1.75) (m^2), h=0.0981 (m), and ε=0.05 (m). The same horizontal spacing of a cell was used for all cases with Δx=0.05 (m) and Δy=0.05 (m).

Figure 2 shows the results of the convergence tests, where N_Z indicates the number of cell used in the vertical between the water surface and seabed. The maximum inlet velocity was obtained from the time series of the jet velocity probed at the position of (x,y)=(0, 0.025m) on the water surface while the third tide was generated at the bay entrance. In the figure, the maximum inlet velocity seems to converge as CFL number decreases independently of the number of cells in the

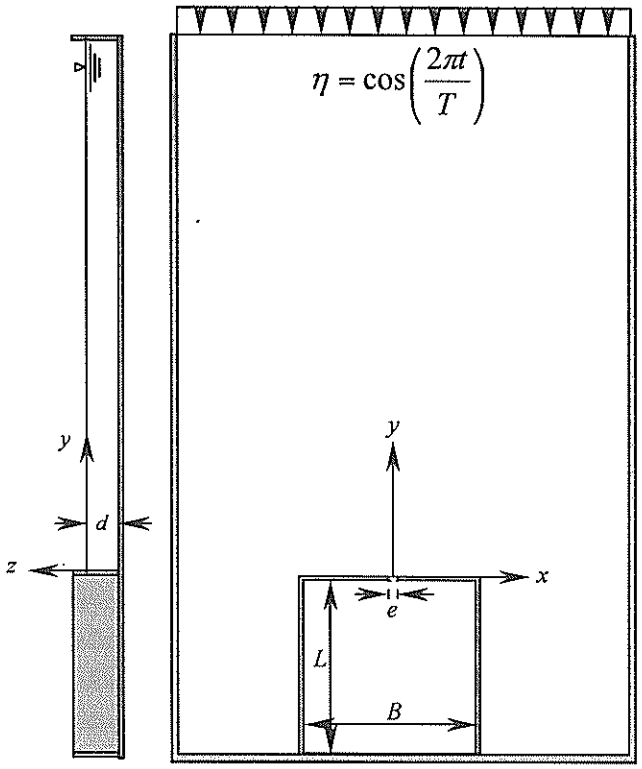

Figure 1 A Tidal-Jet Generator (TJG) Model

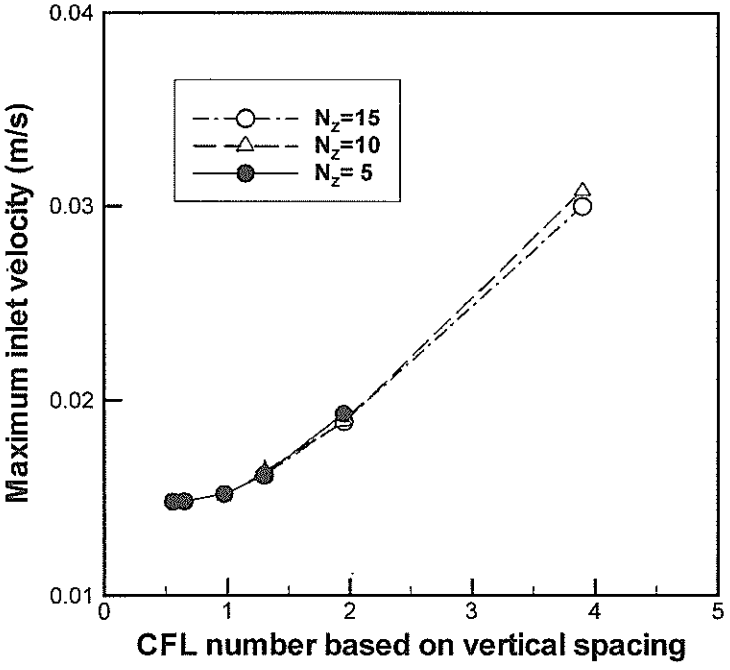

Figure 2 Convergence tests for the numerical model, NS-MAC-TIDE model

vertical, for N_Z between 5 and 15. It is evident from **Figure 2** that the CFL number based on the vertical spacing of a ce should be chosen under 0.5 for the present fully-three dimensional simulation. It is also seen that 5 cells in the vertica are sufficient to define the current flow field. Hereunder, we perform all calculations with 5 cells in the vertical.

In **Figure 3**, the maximum inlet velocity increases with increasing incident tide amplitude. The same tendenc appeared for the relationship to the area of the TJG shown in **Figure 4**.

4.3 Comparison with Other Numerical Methods

Experimental results from previous study (Furukawa et al., 1994) were re-analyzed and a new relationship between th nondimensional maximum intensity of inlet velocity, U_{max}, and the opening ratio, ε_0, was developed. The re-analyze experimental data is presented in **Figure 5**. The empirical function $U_{max}=a/\varepsilon_0$, where a=4/3, was found to fit th experimental data well. The coefficient a represents the ratio of the maximum intensity of inlet velocity generated by th tidal jet to the case where no tidal jet is present. The value of a shows the tidal jet causes the maximum intensity of inle velocity to become 4/3 times larger than when no tidal jet is present. The results computed by the NS-MAC-TIDI method are plotted in **Figure 5**, with the results of the three other independently developed numerical models fo comparison with the experimental results and the empirical relationship. The specific conditions for three numrerica models are listed in **Table 2**. In **Figure 5**, it is apparent that the two fully three-dimensional numerical models NS-MAC-TIDE and CIP-CSF, can predict the maximum intensity of inlet velocity with high accuracy compared with th empirical function. The 3D-ADI and DVM models deviated from the experimental and empirical relationships for smal opening ratio, with ε_0<0.005. The deviation of the 3D-ADI results especially was considerable. It means that as th opening ratio becomes smaller than 0.005 the water level differences between the inner and outer sides of breakwate should be larger and three-dimensional features as like large water falling down and splashing up by tidal jets in th vicinity of the opening cannot be ignored. Then it would be no longer allowed a hydrostatic assumption for pressure in the vertical.

4.4 Flow Characteristics of the Tide-Induced Jets

The tide-induced jets are of significant importance in near-shore zone because they give influences on the transport mechanism of mass and sediment and the distribution mechanism of nutrients. However, there are very few investigations for the three-dimensional flow structure in a periodic tidal motion due to the assumption of hydrostatic pressure in the vertical and of steady jet. In this section, the three-dimensional flow characteristics of the tide-induced jets and their effects will be discussed numerically with the high accuracy of calculation by the NS-MAC-TIDE method.

Table 2 Computational Conditions for Numerical Models

3D-ADI	DVM	CIP-CSF
$\Delta x=\Delta y=0.05$ (m), $\Delta z=h/5$ (m)	578 vortex points positioned at the boundary and 1020 vortex points released into flow	$\Delta x=\Delta y=0.025$ (m) (for minimum size), $\Delta z=h/5$ (m)
CFL number=0.65	Δt=1 (sec)	CFL number=0.43
Horizontal and vertical eddy diffusivity, $\nu_h=3.0\times10^{-2}$, $\nu_z=3.0\times10^{-4}$, respectively	Horizontal eddy viscosity coefficient, $K_X=0.05hU$	Kinematic viscosity, $\nu=1.0\times10^{-}$
Bottom friction coefficient, γ_b=0.05	Bottom friction coefficient, γ_b=0.4	Bottom friction; No-slip condition

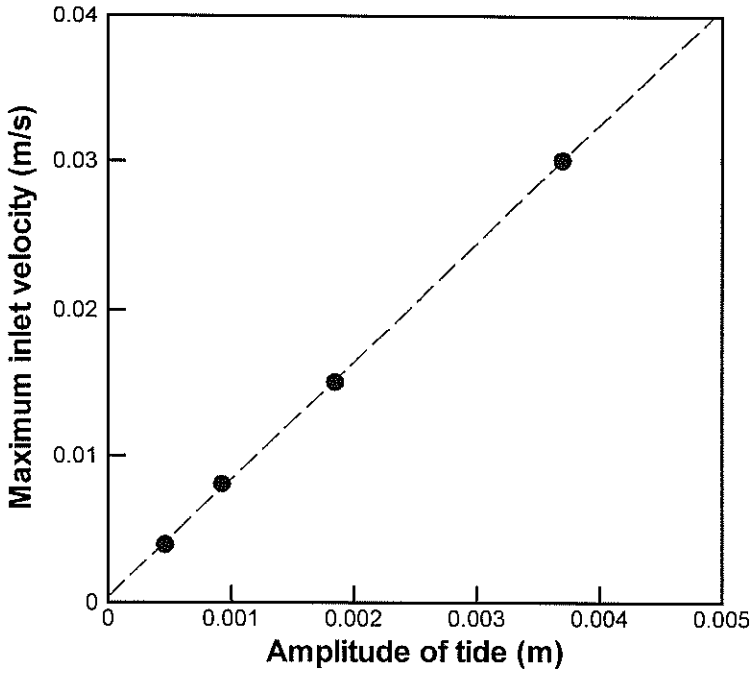

Figure 3 Computed maximum inlet velocity versus amplitude of tide by the NS- MAC-TIDE model

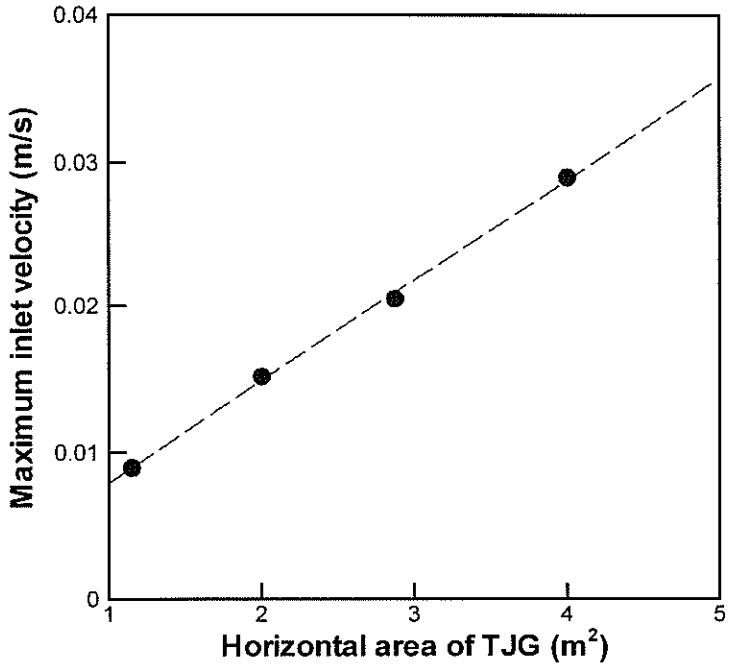

Figure 4 Computed maximum inlet velocity versus horizontal area of the TJG by NS-MAC-TIDE model

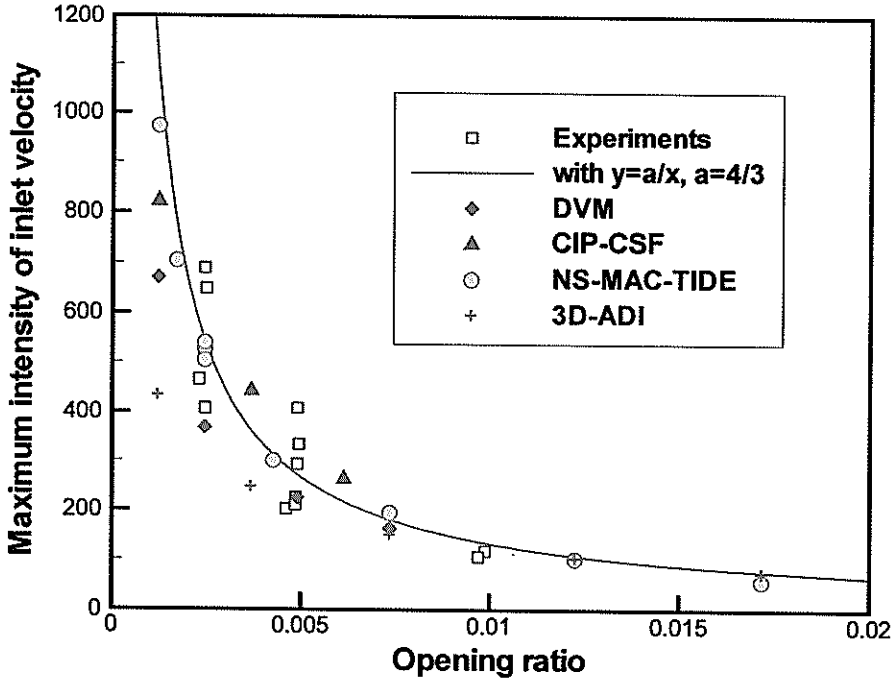

Figure 5 Relationship between maximum intensity of inlet velocity and opening ratio of the TJG

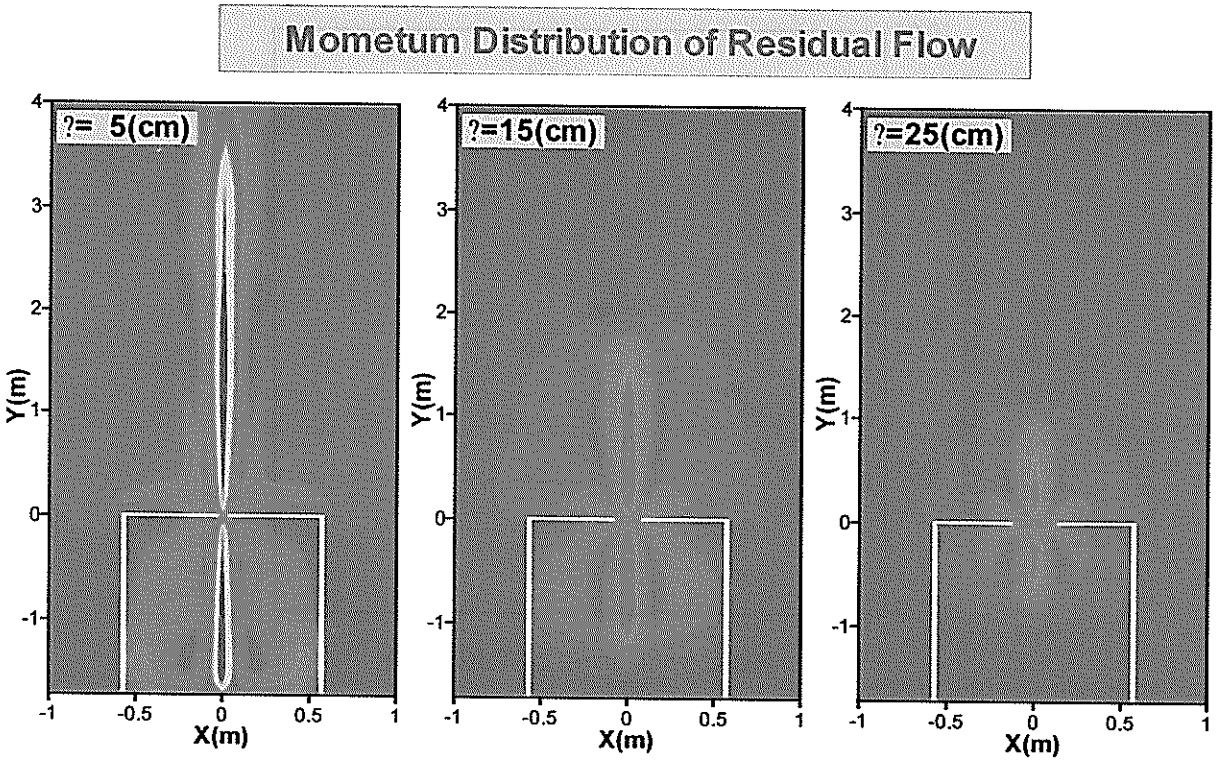

Figure 6 Momentum distribution of residual flow with the three different openings; blue:0 and red:100 (m/s)

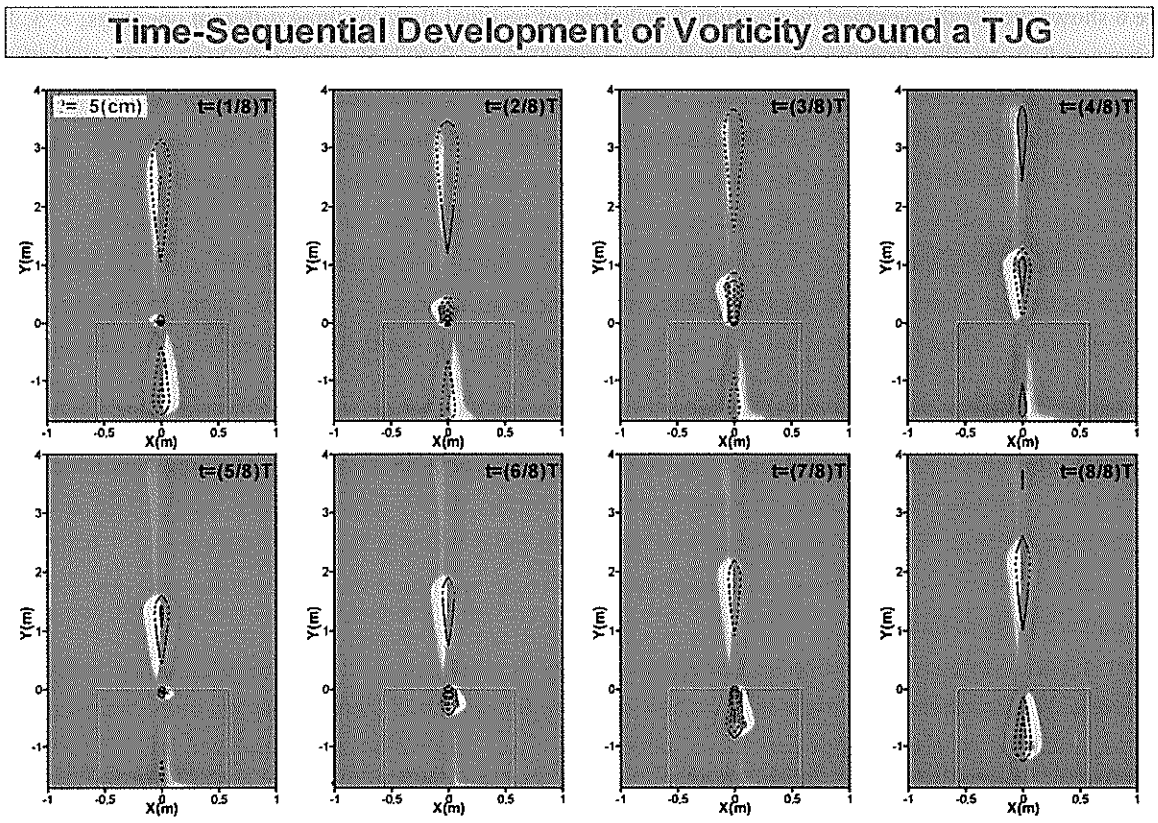

Figure 7 Time-sequential development of tidal jet velocity (dotted lines, interval 0.004 m/s) and jet-induced vortex (flood, blue:0.12/s, red:-0.12/s)

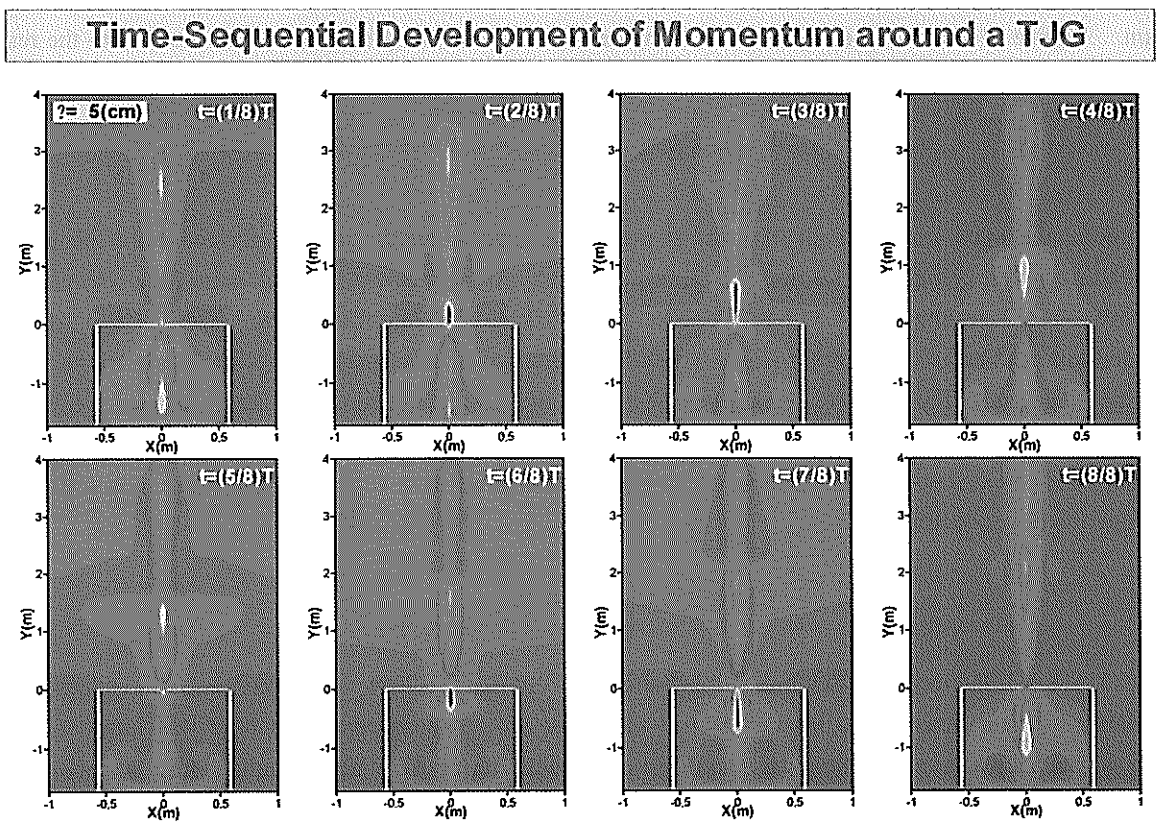

Figure 8 Time-sequential development of momentum around a TJG (blue:0.0 m/s, red:0.012m/s)

Figure 6 shows the depth-averaged momentum distribution of residual flow for three different openings; ε=5, 15 and 25 (*cm*), corresponding to the non-dimensional values; ε_0=0.002453, 0.007358 and 0.012263. The depth-averaged momentum was obtained by taking the absolute value of the residual flow velocity remained during a tidal motion, currently during the third tidal motion. As the opening gets small the momentum is distributed widely and strongly in the vicinity of the TJG, in which the high values are represented in the area where the tidal jet motion is occurred violently.

In order to observe a time- sequential of process of tide-induced jet in detail, let's limit to a consideration of the case of ε=5 (*cm*) onwards. The contour maps for the tide-induced jet velocity and jet-induced vorticities are exhibited during periodic tidal motion in **Figure 7**, and the momentum in **Figure 8**. In the figures each shot is made for one eighth of the incident tide period. In **Figure 7**, the dotted lines indicate the jet velocity and the coloring the vorticity near the water surface. From these figures, it is seen that during both phases of tide the typical processes of the tidal jet are reproduced well numerically, which the jet issued from the inlet induces a pair of large-eddy vortex, entraining the surrounding waters as it proceeds far from the inlet. The jets interact with the vortices causing the dissipation of its momentum gradually.

Figure 9 shows the time-sequential configuration of water surface in the vicinity of the inlet. The local waves are generated through the inlet, and then propagated and dissipated independently with the tidal motion. It may affect the vertical structure of flow field, even though its amplitude and length are much smaller than those of tide given at inflow boundary comparatively in this case.

In **Figure 10**, the vertical distribution of centerline velocity is exhibited as time-sequences. The reflecting wall is located at left and the zone shown at right is at y=2.0 (*m*) in the figure. It is obvious that the numerical simulations can reproduce successfully the processes of generation, development and dissipation of tide-induced jets. For this case, the local Reynolds number caused by the local jet flow at the inlet is estimated at around 7.5×10^2. If the jet flow can be treated as having laminar behavior, the boundary layer thickness from the Blasius solution is approximately 5.8 (*cm*) at the position y=2.0 (*m*), in which the boundary layer occupies about 60% of the water depth.

The vertical structure of velocity and the development of boundary layer near seabed is closely related to the sediment transport, and it is especially important to predict the distribution of shear stress for wide-understanding the transport mechanism. **Figure 11** shows the distribution of computed shear stress along the centerline seabed with the result from the case of ε=15 (*cm*), in which the shear stress was calculated by equation (20):

$$\frac{\tau_B}{\rho} = (\nu + \nu_S)\frac{\partial V}{\partial z}. \tag{20}$$

In the figure, the maximum strength of shear stress is indicated when the jets are formed from the inlet at both maximum ebbing and flooding: t=(1/4)T and (3/4)T, respectively. At the moment, the maximum shear velocity converted from bed shear stress is estimated at 0.35 (*cm/s*) due to the jet formation around the inlet, then the limitations of grain size for suspended load and bed load are approximately 0.065 and 0.0055 (*mm*), respectively (Nichols and Biggs, 1985). By this calculation, the sand drift in suspension may be easier to occur than that in bed load under the current condition.

Finally, in order to investigate the flushing mechanism for water purification and mass transport in front of the TJG, the time-residual rates of concentration are calculated for three openings of ε=5, 15 and 25 (*cm*), solving a following scalar transport equation of concentration C:

$$\frac{\partial C}{\partial t} + \nabla(\mathbf{u}\cdot C) = \left(\frac{\nu + \nu_S}{S_{CH}}\right)\nabla^2 C. \tag{21}$$

In equation (21), S_{CH} is the turbulent Schmidt number chosen as 0.7 (Rodi, 1993), and the concentration C can be assumed like as pollutants, water nutrients or littoral effluent materials etc. The concentration field was introduced after the second tide was generated at inflow boundary, and then computed with the flow field simultaneously at each time-step in the time-marching procedure. Initially the concentration is set at C=1 in the rectangular region located in front of the TJG and at C=0 otherwise, see **Figure 12**. The time rate of concentration residual is calculated by integrating the

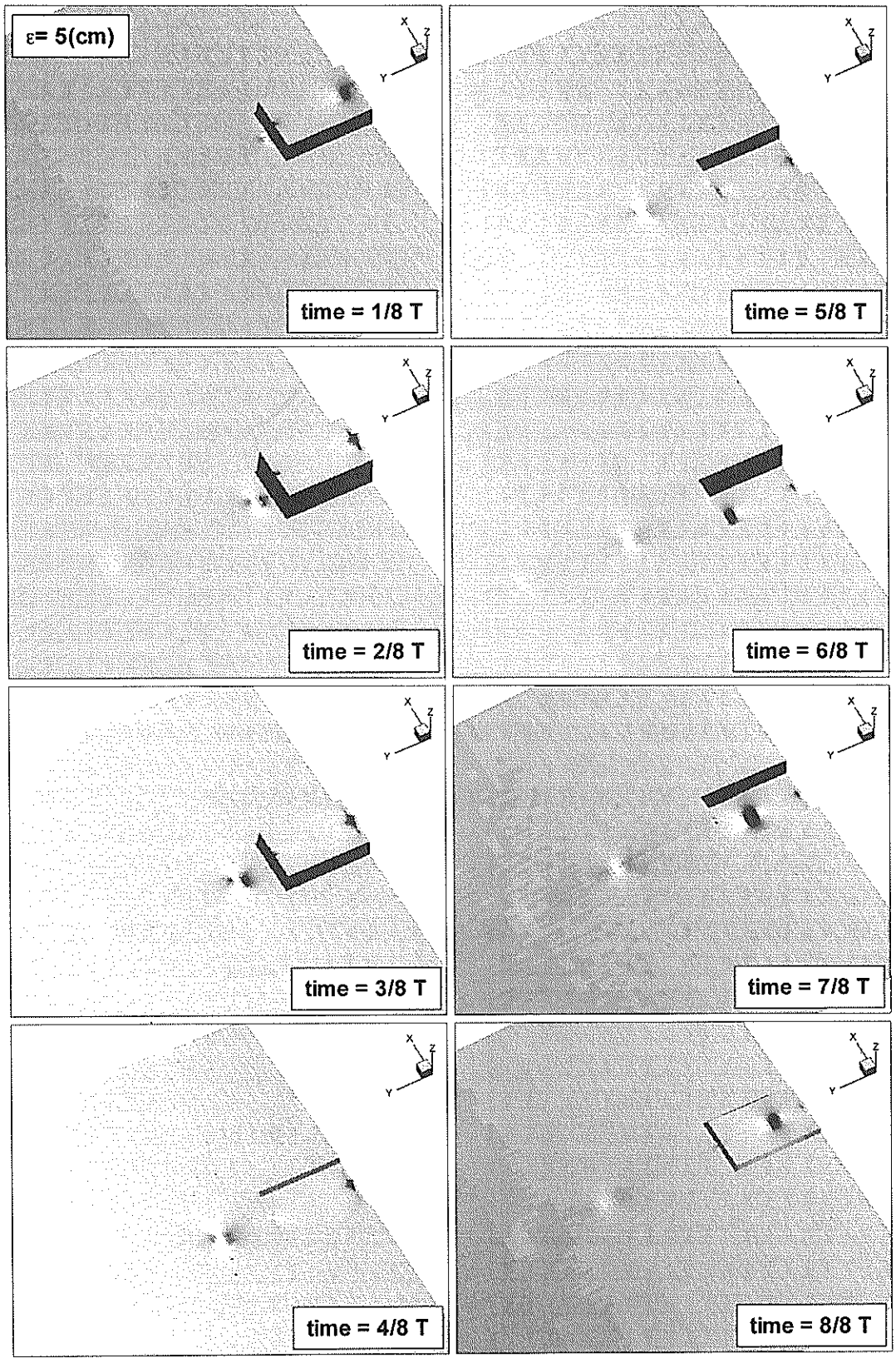

Figure 9 Time-sequential movement of water surface, 40,000 times enlarged on vertical scale

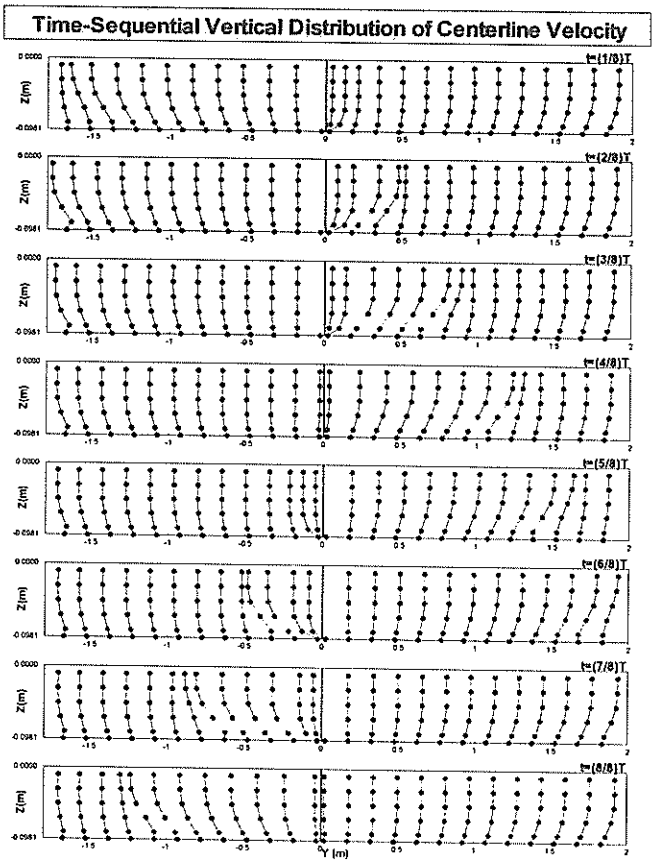

Figure 10 Time-sequential development of vertically-distributed centerline velocity computed by the NS-MAC-TIDE model

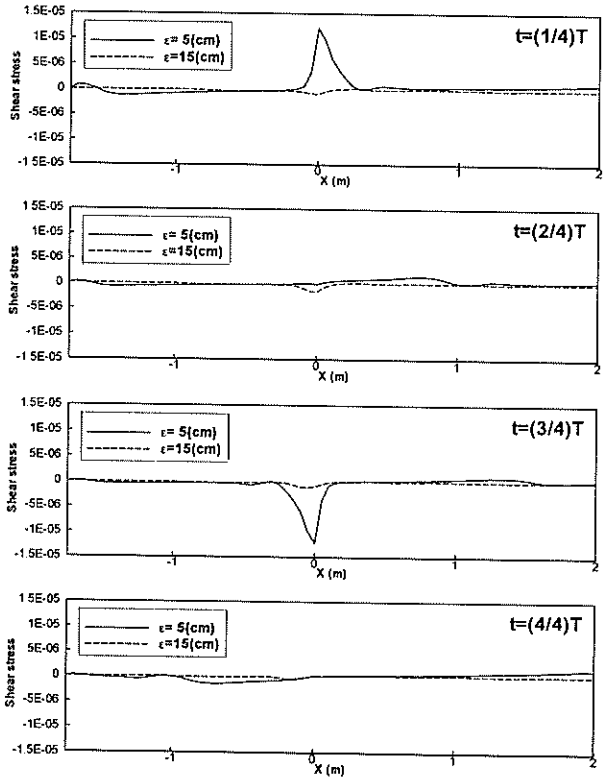

Figure 11 Time-sequential distribution of shear stress along centerline seabed

concentration residual over a whole of the monitored control volume chosen as $2h$ (m^3) equal to the enclosed volume of the TJG, 2 (m^3). The non-dimensional time rate is made by initially obtained value. The time variation of concentration residual is shown in **Figure 13**. During four tidal periods the total proportions of concentration in the control volume are decayed at 52%, 25% and 15% for the cases of ε=5, 15 and 25 (*cm*), respectively. Therefore, the residual time in the monitored area can be estimated approximately about 8T, 16T and 27T, respectively. For the three openings, the instantaneously distributed concentrations on the water surface at different time steps are displayed in **Figure 14**. **Figure 14** shows that for the case of ε=5 (*cm*) the concentration is decayed and flushed away from the inlet remarkably as time increases due to the tidal jet effect, while the other cases indicate the moderate variation. It is verified clearly here that the locally-induced jet flow can decrease the residence time of a pollutant distributed around the outside of inlet, and its effect utilizes tidal energy to influence the local marine environment by providing a flushing mechanism for water purification.

From this study, it seems reasonable to conclude that the NS-MAC-TIDE method presented here simulates well the development of tidal jets and related complicated processes. Fundamentally, however, all the above statements should be treated with caution as all discussed situations are for model-based works, rather than for a real situation.

5. Concluding Remarks

The tide-induced jets over constant bathymetry were investigated in oscillating flow using a finite-difference numerical scheme, named NS-MAC-TIDE based on the fully 3D Navier-Stokes (NS) equations. In order to generate a jet in a tide-like oscillating flow, an enclosed rectangular breakwater, which has vertical opening and a large enclosed volume inside, known as a Tidal-Jet Generator (TJG), was introduced into a flow.

The fully three-dimensional NS-MAC-TIDE simulations are compared with the experiments by Furukawa et al. (1994). The computed results are also extensively compared with three other independently developed numerical models, namely, 3D-ADI, DVM, and CIP-CSF. These models are based on quasi-three-dimensional, two-dimensional depth-averaged and fully three-dimensional NS equations, respectively. It is apparent that the fully three-dimensional numerical models can predict the maximum intensity of inlet velocity with high accuracy compared with the empirical function proposed from the experiment. It seems to be clear that fully three-dimensional fluid motions play an important role to discuss the detailed structure and mechanism in the nonlinear phenomena of coasts. It is also obvious that the numerical simulations can reproduce successfully the processes of generation, development and dissipation of tide-induced jets.

(Received on March 31, 2000)

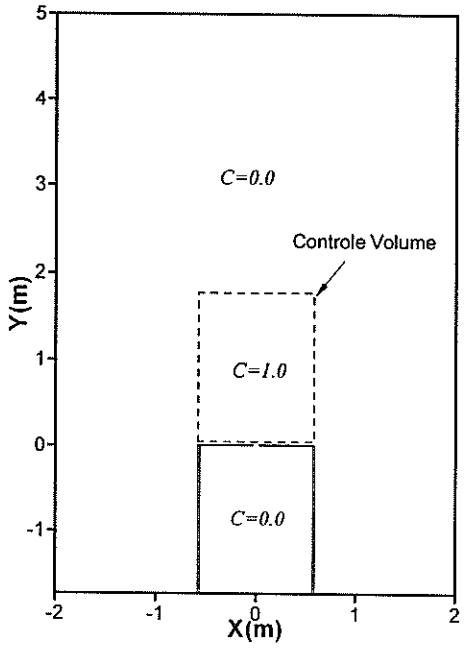

Figure 12 Initial condition for the calculation of concentration transport

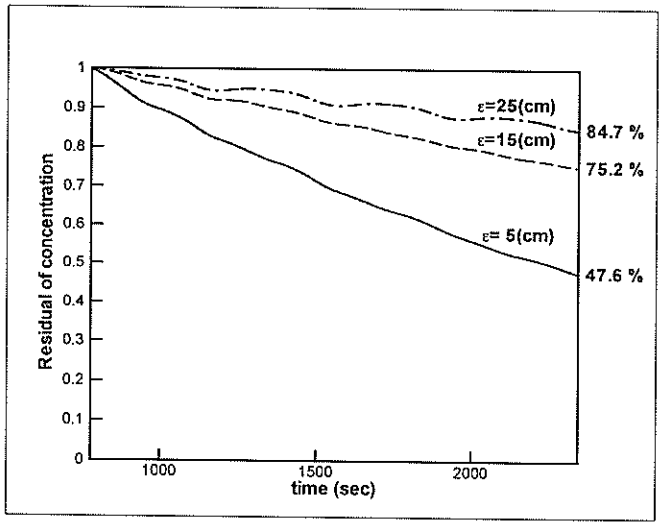

Figure 13 Time evolution of the residual of concentration in a monitored control volume

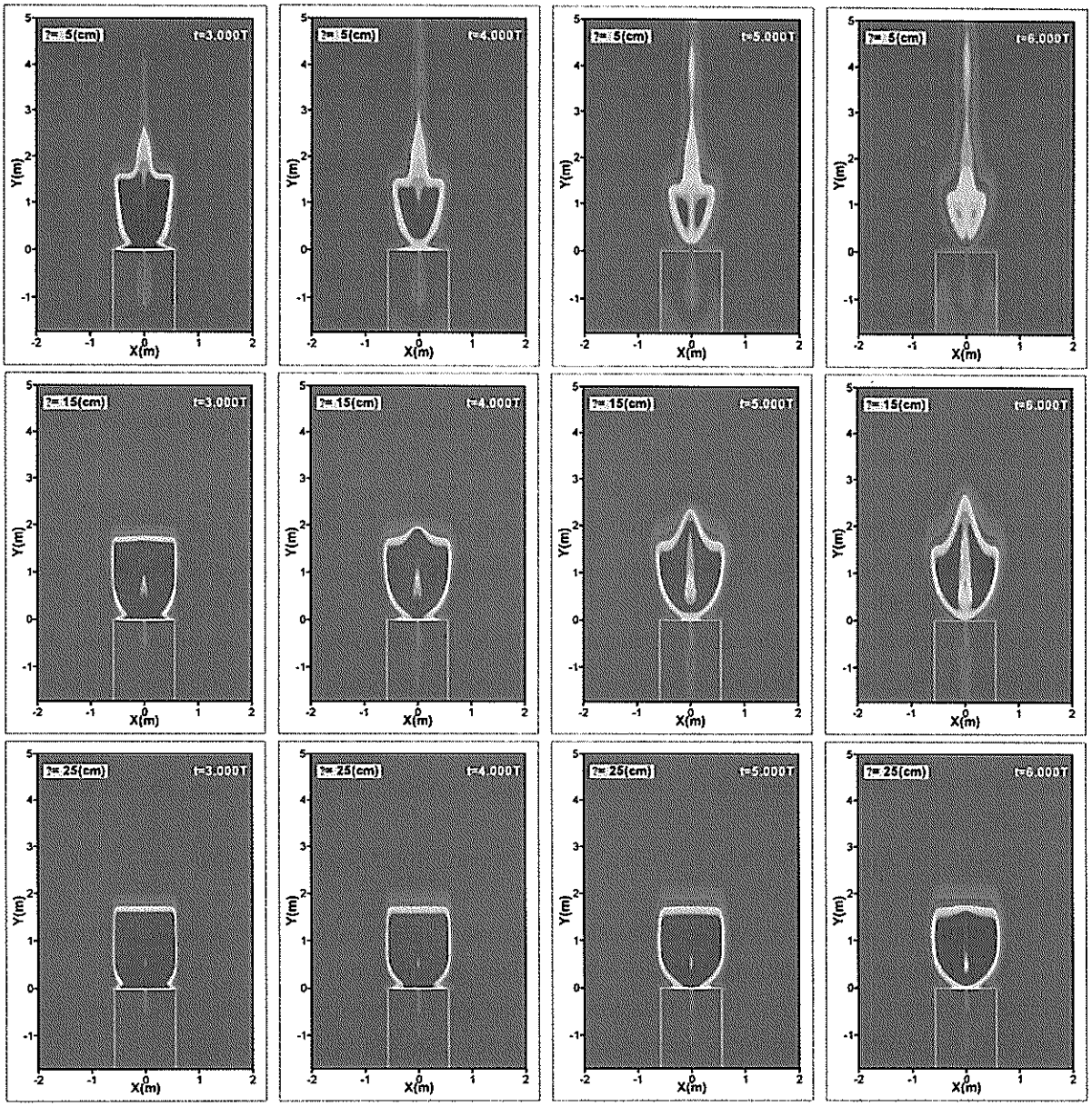

Figure 14 Distribution of the residual of concentration at various time for the cases of *?* = 5, 15 and 25 (*cm*)

References

Chan, R.K.C. and Street, R.L. (1970) : A Computer Study of Finite Amplitude Water Waves, *J. Computational Physics*, Vol.6, pp.68-94.

French, J.L. (1960) : Tidal Flow in Entrances", *Bulletin No.3*, U.S. Army Corps of Engineers, Committee of Tidal Hydraulics.

Furukawa, K., Hirano, T. and Hosokawa, Y. (1994) : Flow Analysis on Tidal Flow Generator –Hydraulic Experimental and Numerical Simulation –, *Report of the Port and Harbour Research Institute*, Japan, Vol.33, No.1, pp.37-66. (in Japanese).

Furukawa, K. and Hosokawa, Y. (1994) : A Three Dimensional Physical–Biological Modeling and its Application to Evaluation of Nitrogen Uptake at Coast, *Report of the Port and Harbour Research Institute*, Japan, Vol.33, No.3, pp.27-56. (in Japanese).

Furukawa, K. and Wolanski, E. (1998) : Shallow -water Frictional Effects in Island Wakes, *Estuarine, Coastal and Shelf Science*, Vol.46, pp.599-608.

Hirt, C.W., Amsden, A.A. and Cook, J.L. (1972) : An arbitrary Lagrangian-Eulerian computing method for all flow speeds, *J. Comp. Phys.*, Vol.14. pp.227-253.

Hirt, C.W., Nichols, B.D. and Romero, N.C. (1975) : SOLA : A numerical solution algorithm for transient fluid flows, *Los Alamos Scientific Laboratory*, report LA-5852.

Ismail, N.M. and Wiegel, R.L. (1983) : Opposing Wave Effect on Momentum Jets Spreading Rate", *J. Waterway, Port, Coastal and Ocean Engineering*, ASCE, Vol.109, No.4, pp.465-483.

Joshi, P.B. (1982) : Hydromechanics of Tidal Inlets, *J. Port, Waterway, Harbor, and Ocean Division*, ASCE, Vol.108, No.WW3, pp.239-253.

Joshi, P.B. and Taylor, R.B. (1983) : Circulation Induced by Tidal Jets, *J. Waterway, Port, Coastal and Ocean Engineering*, ASCE, Vol.109, No.4, pp.445-464.

Kuwahara, K. (1978) : Study of flow past a circular cylinder by an inviscid model, *J. Physics Soc. of Japan*, Vol.45, No.1, pp.292-297.

Leendertse, J.J. (1989) : A New Approach to Three-Dimensional Free-Surface Flow Modeling, *The RAND cooperation*, R-3712-NETH/RC.

Mei, C.C. (1994) : The Applied Dynamics of Ocean Surface Waves, *World Scientific Publishing Co. Pte. Ltd.*, second printing.

Miyata, H. and Park, J.C. (1995) : Ch.5 Wave Breaking Simulation, *Advances in Fluid Mechanics, Potential Flow of Fluids*, ed. M. Rahman, Computational Mechanics Publications, UK., pp.149-176.

Miyata, H. and Yamada, Y. (1992) : A Finite Difference Method for 3D Flows about Bodies of Complex Geometry in Rectangular Co-ordinate Systems, *Int. J. Numerical Methods in Fluids*, Vol.14, pp.1261-1287.

Nakayama, K. and Satoh, T. (1999) : Analysis of Plumes on Horizontal Surface by LES Model, *J. of Hydraulic, Coastal and Environmental Engineering*, JSCE, Vol.628, II-48, pp.97-114 (in Japanese).

Nichols, M.M. and Biggs, R.B. (1985) : Ch.2 Estuaries, *Coastal and Sedimentary Environments*, ed. R.A. Davis, Springer-Verlag, New York, pp.77-186.

Ozsoy, E. (1977) : Flow and Mass Transport in the Vicinity of Tidal Inlets, *Technical Report No.TR-026*, University of Florida, Coastal and Oceanographic Engineering Laboratory.

Park, J.C., Kim, M.H. and Miyata, H. (1999) : Fully Non-linear Free-Surface Simulations by a 3D Viscous Numerical Wave Tank, *Int. J. for Numerical Methods in Fluids*, Vol.29, pp.685-703.

Park, J.C. and Miyata, H. (1994) : Numerical Simulation of the Nonlinear Free-Surface Flow Caused by Breaking Waves, *ASME* FED-, Vol.181, Free-Surface Turbulence, pp.155-168, Lake Tahoe.

Rodi, W. (1993) : *Turbulence models and their application in hydraulics*, 3rd ed., Balkema, Rotterdam, The Netherlands.

Schmidt, H. and Schumann,U. (1989) : Coherent structure of the convective boundary layer derived from large-eddy simulations, *J. Fluid Mech.*, Vol.200, pp.511-562.

Taylor, R.B. and Dean, R.G. (1974) : Exchange Characteristics of Tidal Inlets, *Proc. of 14-th Coastal Engineering Conference*, ASCE, pp.2268-2289.

Unluata, U.A. and Ozsoy, E. (1977) : Tidal Jet Flows Near Inlets, *Hydraulics in the Coastal Zone*, ASCE, New York, pp.90-98.

Wolanski, E., Drew, E., Abel, K.M. and O'Brien J. (1988) : Tidal Jets, Nutrient Upwelling and Their-Influence on the Productivity of the Alga *Halimeda* in the Ribbon Reefs, Great Barrier Reef, *Estuarine, Coastal and Shelf Science*, Vol.26, pp.169-201.

Yabe, T., Takeo, I. and Yusaku, K. (1990) : A multidimensional cubic-interpolated pseudoparticle (CIP) method without time splitting technique for hyperbolic equations, *J. of The Physical Society of Japan*, Vol.59, No.7, pp.2301-2304.